Modulation of Protein-Surface Interactions on Nanopatterned Polymer Films

K. H. Aaron Lau, Joona Bang, Craig J. Hawker, Dong Ha Kim, and Wolfgang Knoll

Supporting information

1. **AFM height images corresponding to the nanopatterns shown in Figure 1 in the main text.**
2. **Surface composition of self-assembled PS-*b*-PMMA**
3. **SPR protein adsorption data**
4. **Image analysis—measuring nanopattern parameters f_{PS}, d_{PS}, and l_{interf}**
5. **References**

1. AFM height images corresponding to the nanopatterns shown in Figure 1 in the main text.

All images show a 1x1 μm^2 scan area. The height scale is 10 nm and the phase scale is 20º. All nanopatterns are considered to have a flat topography relative to the dimensions of the IgG (14 x 9 x 4 nm^3). The nanopatterns with $\lambda_{C\text{-}C}$ < 100 nm exhibited a maximum height difference ~1 nm across the 1x1 μm^2 scan area (Figures S1A and B, and Figure S3), and the larger patterns also exhibited surface curvatures < 0.01 nm^{-1} (e.g., Figure S2C), and maximum height differences ≤ 1 nm over a length scale (50x50 nm^2) that can accommodate several individual proteins (Figures S1C and S2). Therefore all sample surfaces are considered flat relative to the dimensions of the IgG

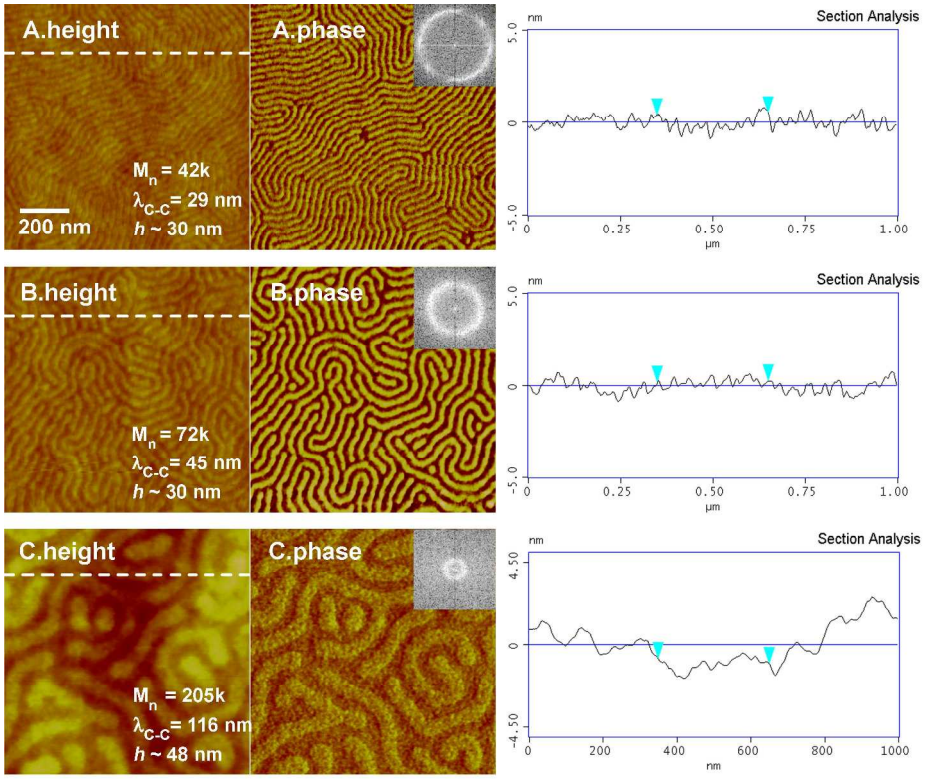

Figure S1. Tapping mode AFM height, phase and cross-section measurements of striped surface nanopatterns self-assembled from PS-*b*-PMMA with approximately 1:1 block volume ratios. The height scale is 10 nm and the phase scale is 20º. All images show a 1x1 μm^2 scan area. As discussed in the text, PS surfaces appear as darker areas in the phase measurement. (A), (B) and (C) differ in the M_n (in g/mol) of the sample. The greyscale insets show the fast fourier transforms of the phase

images, from which $\lambda_{C\text{-}C}$ was measured. The white dashed lines in the height data indicate where the cross-sections were taken along.

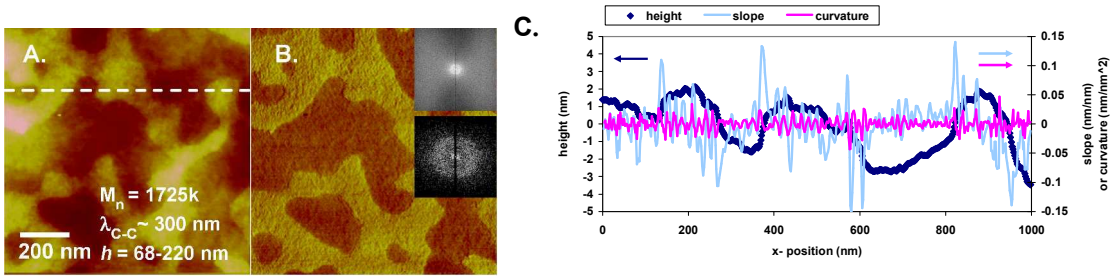

Figure S2. Tapping mode AFM height (A), phase (B) and cross-section (C) measurements of the PS-*b*-PMMA (total M_n = 1725 kg/mol) surface nanopattern (1x1 μm^2 ; height scale = 10 nm; phase scale = 20º). PS surfaces appear as darker areas in the phase measurement. The white dashed line in (A) indicates where the cross-sections (C) was taken. The grayscale insets show the fast fourier transforms of the phase image (measured from the original data scanning a 5x5 μm^2 area), from which $\lambda_{C\text{-}C}$ was measured. The lower FFT is an expanded, contrast enhanced view of the upper inset. (C) shows also the local slope and curvatures along the cross section.

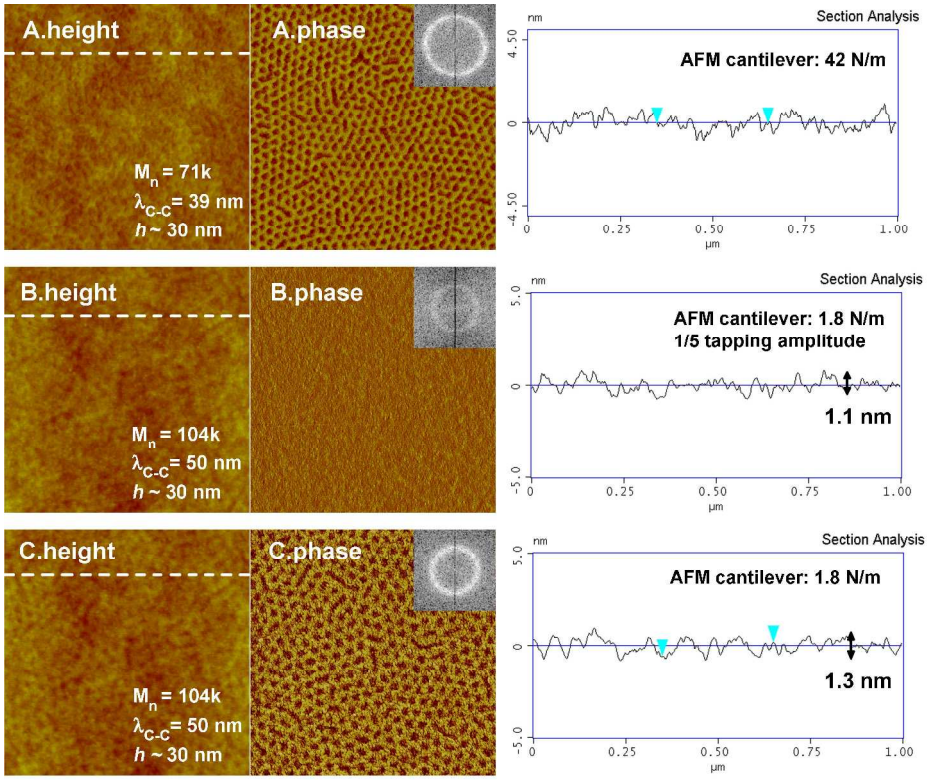

Figure S3. Tapping mode AFM measurements (1x1 μm^2) of surface nanopatterns with hexagonally ordered PS domains, self-assembled from PS-*b*-PMMA with approximately 3:7 block volume ratios. (Height scale is 10 nm; phase scale is 20º.) PS surfaces appear as darker areas in the phase measurement. (A) shows a sample with M_n = 71 kg/mol, while (B) and (C) show samples with M_n = 104 kg/mol. In (B) and (C), different forces were used for the measurements (as indicated in the section analysis on the right), and resulted in different heights in the topography measured and different phase contrast between PS and PMMA domains, but the lateral dimensions remained unaffected. The greyscale insets show the fast fourier transforms of the phase images, from which $\lambda_{C\text{-}C}$ was measured. The white dashed lines in the height data indicate where the cross-sections were taken.

2. Surface composition of self-assembled PS-*b*-PMMA

The surface energies of PS and PMMA at the air interface differ by less than 0.3% (0.1 dyn/cm).[1, 2] Given a substrate with also balanced interfacial energies[3], PS-*b*-PMMA self-assembly in air (or in vacuum) should proceed with no preferential interaction at both the air and substrate interfaces for both PS or PMMA blocks. That is, under such conditions, PS-*b*-PMMA would self-assemble with morphologies oriented normal to the surface and exhibit surface nanopatterns with both PS and PMMA microdomain surfaces exposed.[2] In other words, unlike other block copolymer thin films, such as PS-*b*-PtBA,[4] no skin layers should be formed during the self-assembly of PS-*b*-PMMA in air (or in vacuum).

Tapping mode AFM phase measurements are frequently used to characterize block copolymer nanopatterns. It measures the difference in energy dissipation of the tapping AFM tip on different polymers.[5-7] However, because the tip interaction volume extends a few nanometers below the sample surface, the technique is not sensitive to the presence of skin layers. Although, as discussed above, skin layers are not expected on PS-*b*-PMMA nanopatterns, we verified the nanopattern data gathered from AFM phase measurements by comparing them with lateral force AFM measurements. This latter technique reveals differences in surface composition by sensing differences in the frictional force encountered by a scanning AFM tip in contact with the surface. Lateral force AFM operating under low contact force conditions can be uniquely surface sensitive, and has been used to map, e.g., chemical patterns of different self-assembled monolayers differing only in the surface head group.[5, 8]

We found excellent agreement between the nanopattern data measured by tapping mode phase and lateral force AFM measurements, thus verifying that the phase images shown in Figure 1 in the main text truly reflect chemically heterogeneous surface nanopatterns. Although lateral force AFM could not identify the chemical purity of the PS and PMMA domains, nanopatterns with differentiated (and relatively uniform) surface properties were revealed. Chemical compositions may be verified by, e.g., grazing angle XPS or TOF-SIMS, but the nanoscale resolution relevant to our investigation is lost with such techniques.

As example, Figure S4 compares the images taken by the two techniques for PS-*b*-PMMA nanopatterns corresponding to Figures 1C and 1F in the main text. We also found that lateral force AFM data has a lower signal-to-noise ratio in our measurements, and a higher uncertainty in the nanopattern parameters measured. Figure S5 compares the surface fractions and surface interface boundary densities measured from images obtained by the different techniques.

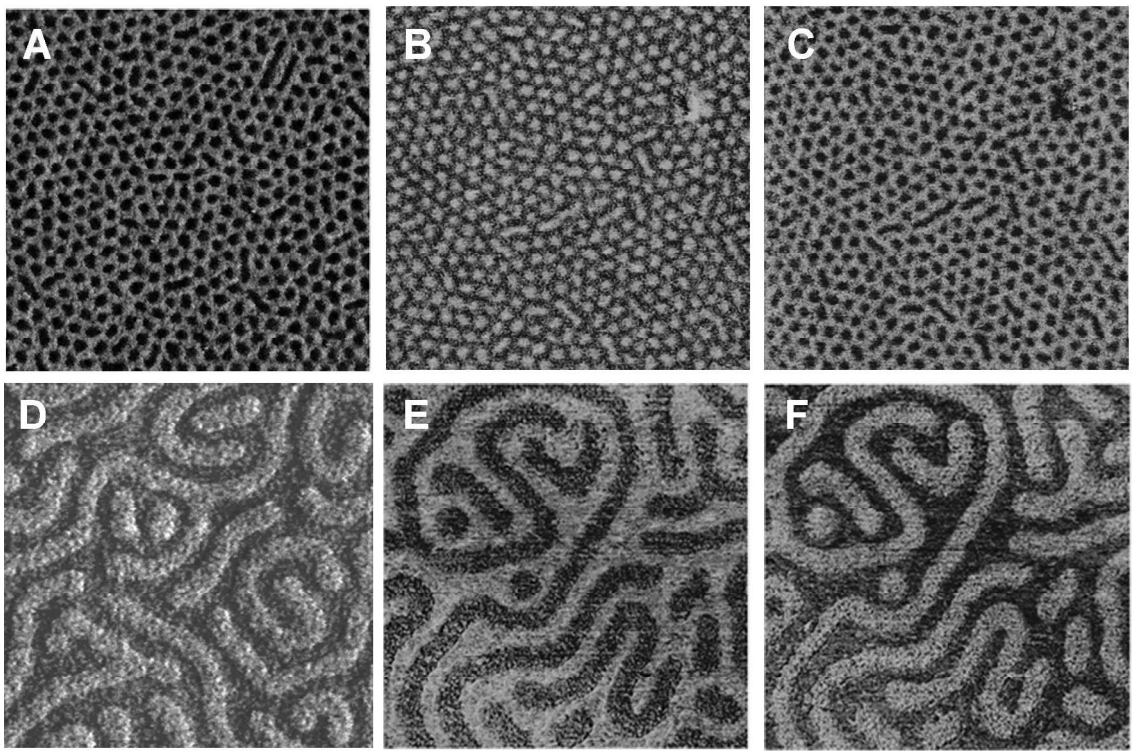

Figure S4. PS-*b*-PMMA nanopatterns revealed by AFM phase and lateral force measurements. (A)-(C): Measurements on PS-*b*-PMMA with M_n = 104k g/mol. (D)-(F): on PS-*b*-PMMA with M_n = 205k g/mol. (A),(D) are phase measurements. (B),(E) are lateral force images measured as the AFM tip was scanned from right to left; (C),(F) were measurements for scans from left to right.

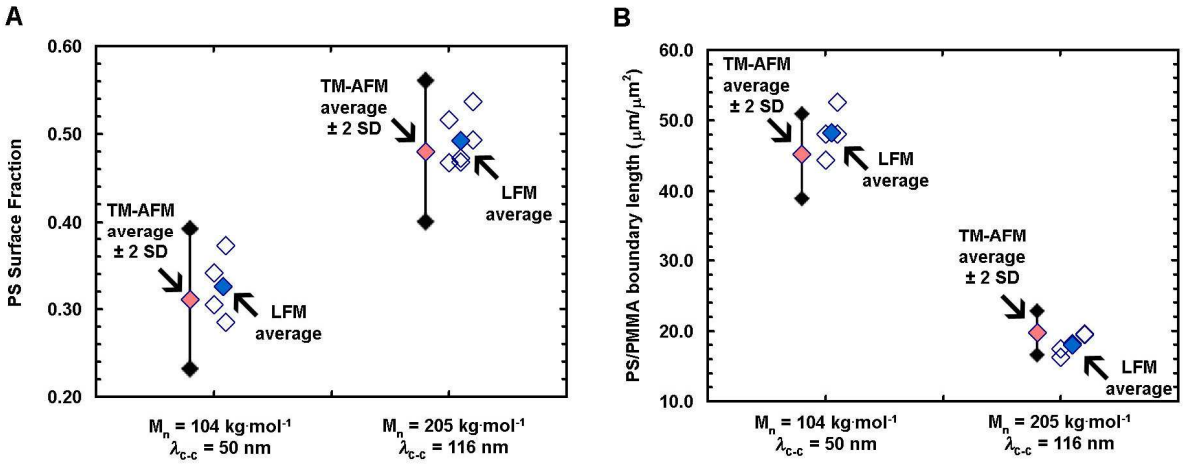

Figure S5. Comparison of PS surface fraction and boundary length measured by tapping mode and lateral force AFM.

3. SPR adsorption data

In situ protein adsorption was measured by reflectivity (R) tracking of the SPR minimum (θ_{SPR}).[9] The incidence angle (θ) was fixed at an angle to the left of θ_{SPR} in the middle of the pseudo-linear region of the R vs. θ scan, and R was recorded in real time with a time-resolution of 5s. As θ_{SPR} shifts to the right to higher incidence angles ($\Delta\theta_{SPR}$) due to protein adsorption (increased optical density on the surface), there is a corresponding increase in R at the chosen angle, since the slope of R vs. θ in this psuedo-linear region is negative. The θ_{SPR} shift is directly proportional to the change in R if the shape of the R vs. θ curve is constant, which is the case when the increase in layer thickness is smaller than 20~50 nm, as is for the present experiment. $\Delta\theta_{SPR}$ is related to the adsorbed protein layer thickness (h) via the protein's refractive index (n) by Fresnel calculations, and $\Delta\theta_{SPR}$ is directly proportional to h, also for thin layers smaller than 20~50 nm. We take a value of n = 1.53 of dried protein layers for our calculations.[10] However, the proteins adsorbed are non-compact and non-spacing filling objects. They are also adsorbed from random orientations, and are solvated to a great extent by water/PBS. Thus h calculated from n = 1.53 is only an effective „dry" layer thickness, and is smaller than would be expected from the dimensions of the protein. In comparison, the refractive index of a „wet" layer of adsorbed IgG (i.e. a layer consisting of both protein and buffer) has been measured to range from 1.38 to 1.42, depending on the material composition of the adsorption surface.[10] However, the mass density of protein adsorbed is not affected by the filling geometry of the protein layer, or by the value of the n used. This is because in the thin film region (thin relative to the wavelength of the probe laser λ = 633 nm), an underestimated n would give an overestimated, but inversely proportional, h, and vice versa. The mass density is calculated from h and n by de Feijter's formula, using a protein refractive index increment (dn/dC) of 0.182 cm^3/g:[10]

$$\text{mass density} = h \frac{n - n_{buffer}}{dn/dC}$$

where n_{buffer} was measured to be 1.333.

Protein adsorption data used to derive Figure 2 in the main text is given below in Figures S6 and S7. As described in the paper, $\Gamma_{norm.}$ was taken for the amount of proteins adsorbed at 180 min for consistency. $\Gamma_{norm.}$ calculated from adsorbed amounts after rinsing showed the same general trend in enhanced adsorption at high surface interface densities. Furthermore, Figure S8 shows the adsorption experiment on a random copolymer P(S-*r*-BCB-*r*-MMA). This is the copolymer used for balanced PS and PMMA interfacial energies, which has a styrene:benzocyclobutene(BCB):MMA fractional composition of 56:2:42. After crosslinking of the BCB component, the sample is considered to have a styrene:MMA ratio of 58:42 due to the similarity in molecular structure between PS the the reacted BCB.

Figure S6 to S8 shows relatively slow adsorption kinetics, which is attributed to bulk diffusion limitations. As discussed in the main text, rinsing effects have been found to induce serious artifacts for interpreting adsorption processes along interfaces of nanopatterned surfaces. Therefore in our experiments, once the protein solution was injected into the liquid flow cell for the in situ SPR measurements (the same flow cell was used for all experiments), the protein solution within the cell was left undisturbed until the end of the adsorption step. Transport of proteins to the surface therefore relied strictly on diffusion. Thus the initial adsorption kinetics appeared slow. Our flow cell chamber is cylindrical in shape and had a thickness of 6 mm and a diameter of 7 mm. This represents quite a large

volume of protein solution for adsorbing monolayers of proteins and the adsorption process, although slow, was not limited by the amount of proteins present in the solution.

The amounts of proteins adsorbed layers shown in Figures S6 to S8 are clearly marked as the effective thickness on the left axes, which corresponds to a "dry", solid protein layer. As already described in the technical description of the SPR technique above, the effective thickness is always thinner than the actual inhomogeneous protein layer, which consists of both the adsorbed proteins and the buffer surrounding them. Moreover, the effective thickness for adsorbed IgG should be compared against the IgG's shortest axis, which is 4 nm. This is because a protein can be expected to preferentially adsorb "flat" on a strongly adsorbing surface such as PS, so as to maximum its interaction with the surface. This implies that the protein would adsorb with its longest axes parallel to the surface and protrude from the surface with its shortest side up (i.e. ~4 nm[11, 12]). Furthermore, the protein may be expected to unfold and flatten itself against the surface to further maximize the protein-surface interaction. Therefore the effective dry-layer thickness of 0.5~2 nm shown in Figures S6 to S8 actually represent rather a reasonable figure—a more intuitive comparison between the measured protein layer and the native protein's size may be inferred from the adsorbed surface mass density instead. The measured mass density are between 0.5~2 ng/mm^2 (Figures S6 to S8, right axes), which can be compared with a theoretical maximum of 2.2 ng/mm^2 or 7.8 ng/mm^2 (or equivalently 123 or 34 nm^2),[13] depending on whether the adsorbed IgG adopts the "flat" or "standing" orientations, respectively. Therefore, relative to the "flat" adsorbed orientation, the measured IgG layers actually corresponded roughly to between a quarter to full surface coverage of a "flat" monolayer.

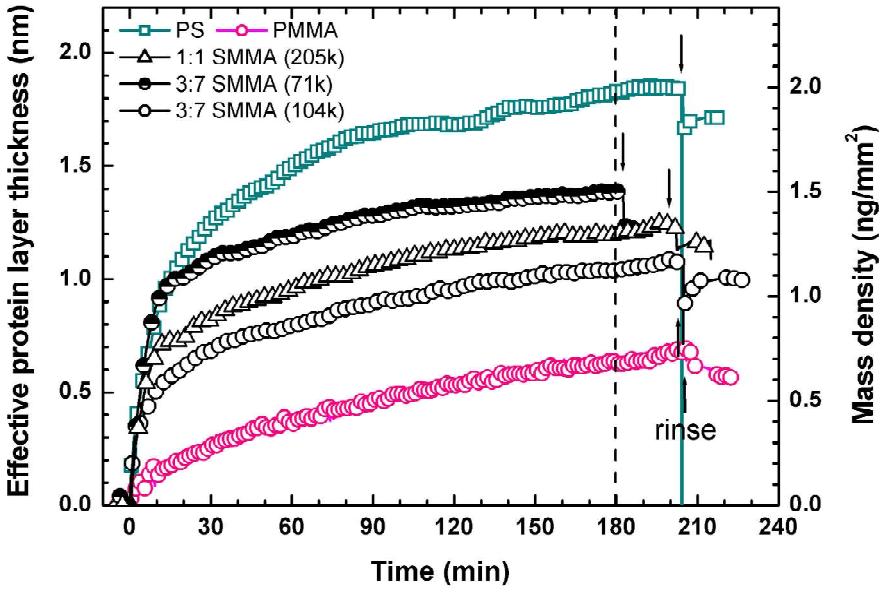

Figure S6. MxG-IgG adsorption on PS, PMMA and nanostructured BCP surfaces. The amount adsorbed at 180 min is indicated by the vertical dashed line.

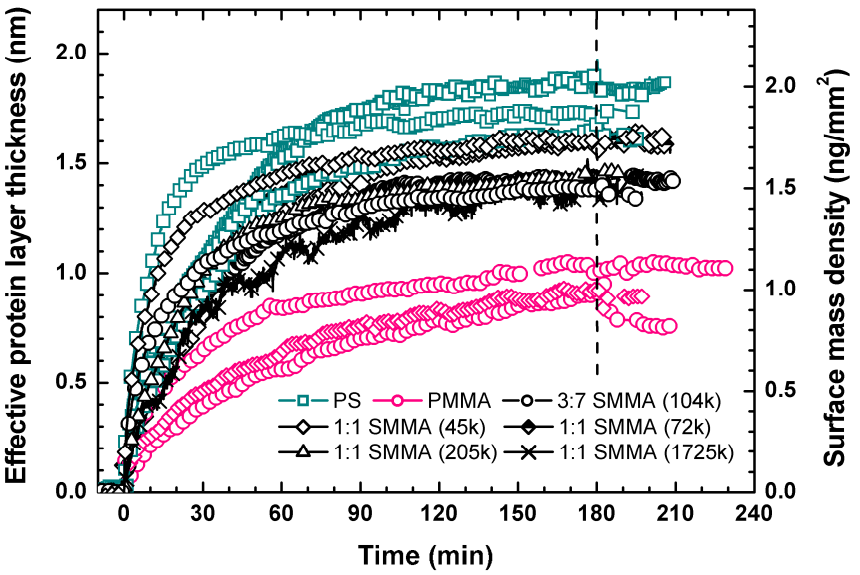

Figure S7. Biotinylated GxR-IgG adsorption on PS, PMMA and nanostructured BCP (SMMA) surfaces. The amount adsorbed at 180 min is indicated by the vertical dashed line. Adsorption on all surfaces except two, the 1:1 SMMA's at 72 and 1725 kg/mol, were repeated to establish the uncertainties of the experiment. The results are clearly repeatable within the bounds of experimental uncertainty. Two distinct sets of initial adsorption rates can be observed, probably due to the difference in geometries of the two teflon liquid cells used. Nonetheless, the final adsorbed amounts were consistent throughout. The protein solutions were not disturbed once injected into the cells, and the adsorptions were performed in a diffusion-limited regime for all experiments shown in Figures S6 to S8.

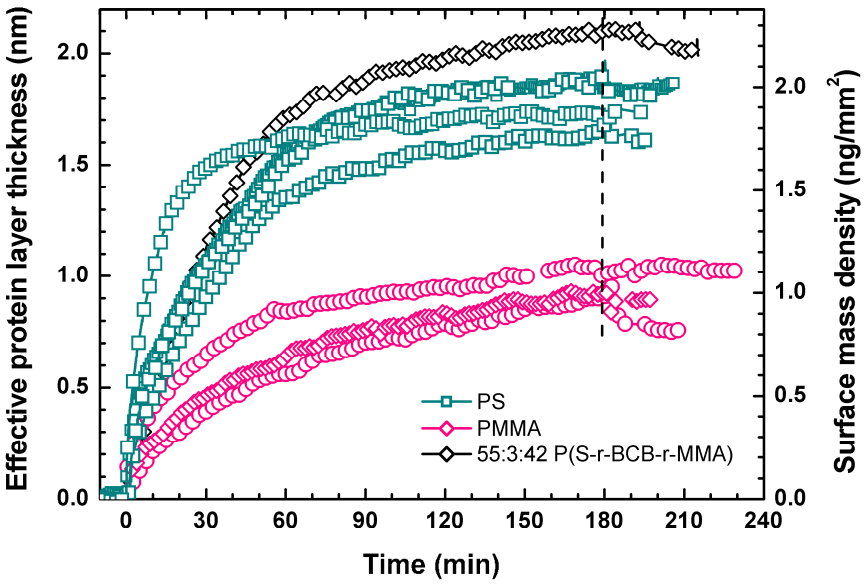

Figure S8. Biotinylated GxR-IgG adsorption on the random copolymer P(S-*r*-BCB-*r*-MMA) (the same as used for balanced PS and PMMA interfacial energies) shown alongside adsorption on PS and PMMA surfaces. The amount adsorbed at 180 min is indicated by the vertical dashed line.

4. Measuring PS-*b*-PMMA nanopattern parameters: f_{PS}, d_{PS}, l_{interf}.

Analysis was based on the phase contrast of PS and PMMA domains in tapping mode AFM phase images. As discussed in the text, PS domains appear as regions darker in shading (lower phase offset) than PMMA regions. Thus the first and key step in identifying the PS domains (or equivalently the PMMA domains) was to set a threshold shading level that corresponded to the spatial extent of PS domains in a phase image. This threshold level was determined from the histogram representation of the phase data, which is obtained from the AFM controller software (NanoScope III software version 5.30r1, 2004). The actual thresholding was done using the "Threshold" function in ImageJ (Rasband WS: Imagej. U. S. National Institutes of Health, Bethesda, Maryland, USA; freely available at http://rsb.info.nih.gov/ij/). Figure S9 illustrates this process with the example of the PS-*b*-PMMA sample (with a PS:PMMA volume ratio of 30:70) corresponding to Figure 1E.

The phase offset histogram plots the number of data points corresponding to each phase offset level. Thus if there are two distinct types of domains in the phase measurement (distinctly darker and lighter shaded domains), corresponding to two types of materials (i.e. PS and PMMA in the present case), they can be identified by their histogram peaks (or histogram clusters). The larger the peak, the more data points correspond to that type of domain, and the larger the surface fraction in the AFM image is composed of that material. Accordingly, the histogram of the phase data corresponding to the nanopatterned PS-*b*-PMMA surface shows a bimodal distribution; the smaller peak corresponds to PS and the larger peak corresponds to PMMA (Figure S9A). For imageJ analysis, the AFM phase data is first exported as a bitmap of greyscale values (levels 0 to 255) by the AFM controller software (NanoScope III software version 5.30r1, 2004). The "Threshold" filter is then used for identifying the domains, and the threshold level was set at the point of overlap between the tails of the two histogram peaks. This is the method of histogram cluster thresholding at minimum overlap,[14] which may be considered to be more accurate than, e.g. thresholding according to the pixel count minimum in the histogram between the histogram cluster peaks, since the error of classifying a background pixel (darker PS) as a foreground pixel (lighter PMMA), or vice versa, is minimized. Also, the threshold level is set globally, not locally. However, an improvement in the accuracy of the image segmentation procedure derived from local thresholding is not expected to be significant in the present case, because the phase images of our topographically flat nanopatterns show a relatively uniform background. More sophisticated techniques, such as edge detection or entropy-based methods were not considered due to the relatively high contrast and simple image compositions of the phase data.

Figure S9B illustrates how the threshold level controls the selection of the pixels corresponding to the PS regions in the image, and Figure S9C shows the resulting black and white image after application of the threshold filter. Finally, the black PS domains can be counted and measured by the "analyze particles" routine in ImageJ (Figure S9D). The domain parameters are defined as follows: 1) f_{PS}: the PS surface fraction is the ratio between the aggregate number of all pixels corresponding to the PS domains and the number of pixels comprising the entire image gives; 2) l_{interf}: the PS/PMMA surface

interface density is the sum of the length of the domain perimeters, relative to the AFM image magnification; and 3) d_{PS}: the characteristic width of the domains is a) for dot patterns, the modal average of the domain diameters, and b) for stripe patterns, the average domain width manually measured from line cross-sections of the phase image.

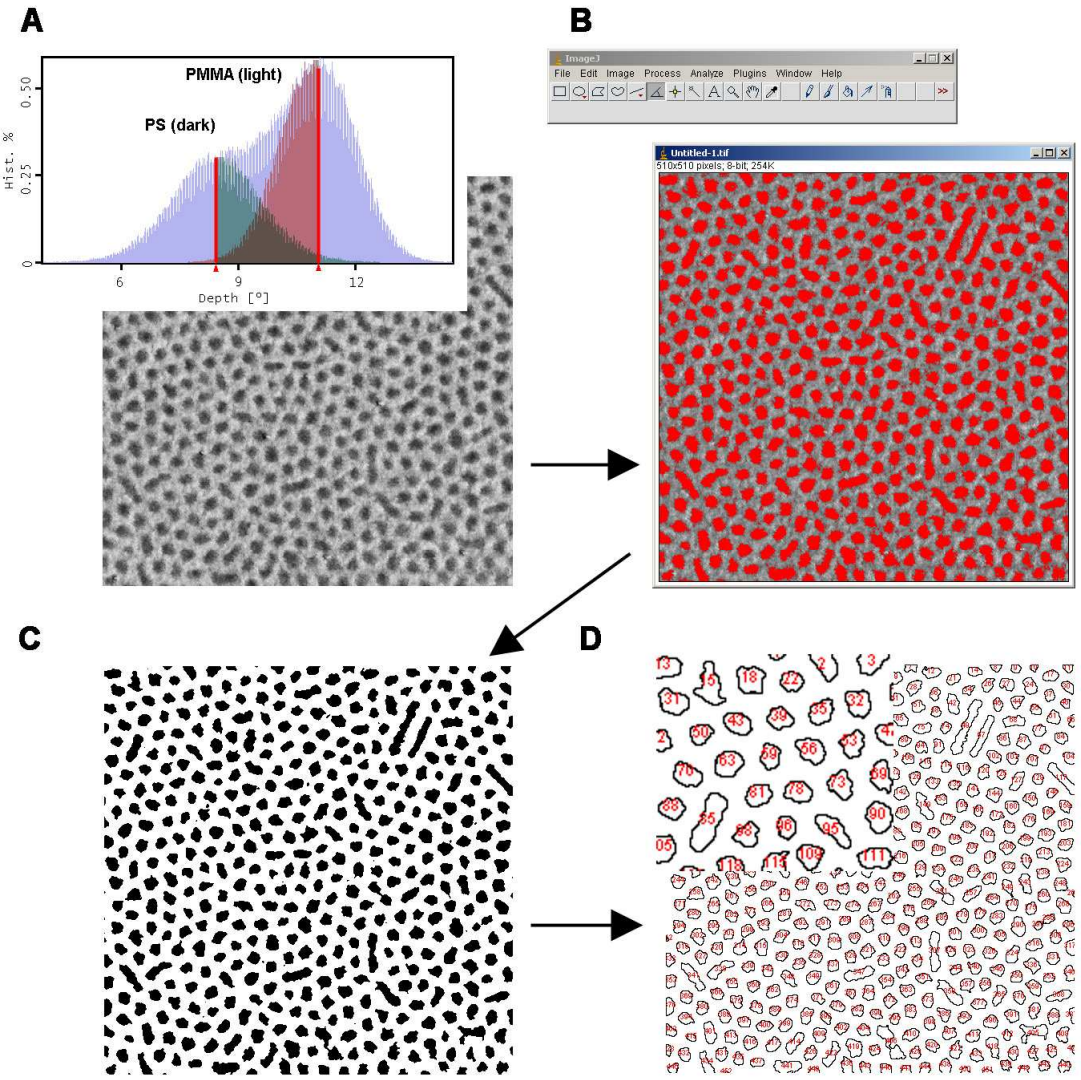

Figure S9. Computer image analysis of AFM phase measurement with ImageJ (3:7 PS-*b*-PMMA sample corresponding to Figure 1E). (A) shows the phase offset histogram of the original AFM measurement, the thresholding level corresponding to the overlap between the tails of the peaks, and the equivalent greyscale image converted from the AFM phase data. (B) shows the image opened in ImageJ and the identified domains. The PS domains are identified in red. (C) shows the resulting black and white image after application of the threshold filter (black now identifies PS), and (D) shows the domains identified, counted and measured by the "analyze particles" routine.

5. References

(1) Brandrup, J.; Immergut, E. H.; Grulke, E. A., *Polymer Handbook*. 4th ed.; Wiley-Interscience: 1999.
(2) Kim, H.-C.; Russell, T. P. *J. Polym. Sci., Part B: Polym. Phys.* **2001**, *39*, 663-668.
(3) Ryu, D. Y.; Shin, K.; Drockenmuller, E.; Hawker, C. J.; Russell, T. P. *Science* **2005**, *308*, 236-239.
(4) Feng, C. L.; Vancso, G. J.; Schonherr, H. *Langmuir* **2005**, *21*, 2356-2363.
(5) Magonov, S. N.; Reneker, D. H. *Annu. Rev. Mater. Sci.* **1997**, *27*, 175-222.
(6) McLean, R. S.; Sauer, B. B. *Macromolecules* **1997**, *30*, 8314-8317.
(7) Wang, H.; Djurišić, A. B.; Chan, W. K.; Xie, M. H. *Appl. Surf. Sci.* **2005**, *252*, 1092-1100.
(8) Sadaie, M.; Nishikawa, N.; Kumashiro, Y.; Ikezawa, Y.; Kumagai, Y.; Makino, K.; Ohnishi, S.; Tamada, K.; Hara, M. *Jpn. J. Appl. Phys.* **2007**, *46*, 7838-7845.
(9) Knoll, W. *Annu. Rev. Phys. Chem.* **1998**, *49*, 569-638.
(10) Voros, J. *Biophys. J* . **2004**, *87*, 553-561.
(11) Xu, H.; Zhao, X. B.; Grant, C.; Lu, J. R.; Williams, D. E.; Penfold, J. *Langmuir* **2006**, *22*, 6313-6320.
(12) Harris, L. J.; Larson, S. B.; Hasel, K. W.; Day, J.; Greenwood, A.; McPherson, A. *Nature* **1992**, *360*, 369-372.
(13) Lynch, M.; Mosher, C.; Huff, J.; Nettikadan, S.; Johnson, J.; Henderson, E. *Proteomics* **2004**, *4*, 1695-1702.
(14) Sonka, M.; Hlavac, V.; Boyle, R., *Image Processing, Analysis, and Machine Vision*. 3rd ed.; Cengage Learning: Florence, 2007.